The 8th International Supercritical CO_2 Power Cycles Symposium
February 27 – 29, 2024, San Antonio, Texas
Paper #113

COATED AND UNCOATED STEEL COMPATIBILITY IN SUPERCRITICAL CO_2 AT 450°-650°C

Bruce A. Pint
Group Leader
Oak Ridge National Laboratory
Oak Ridge, TN 37831-6156 USA
pintba@ornl.gov

Rishi Pillai
Senior R&D Staff Member
Oak Ridge National Laboratory
Oak Ridge, TN 37831-6156 USA
pillairr@ornl.gov

Michael J. Lance
Group Leader
Oak Ridge National Laboratory
Oak Ridge, TN 37831-6156 USA
lancem@ornl.gov

James R. Keiser
Distinguished R&D Staff Member
Oak Ridge National Laboratory
Oak Ridge, TN 37831-6156 USA
keiserjr@ornl.gov

Bruce Pint is the interim section head for Materials in Extremes in the Materials Science & Technology Division at ORNL. For 15 years he was the group leader of the Corrosion Science & Technology Group in the section. He received his Ph.D. from M.I.T. in Ceramic Science and Engineering in 1992 and has been at ORNL since 1994. His research covers compatibility, lifetime predictions, environmental effects and coatings in all types of power generation. He is a Fellow of NACE International and ASM International and is the Associate Editor for the journal High Temperature Corrosion of Materials.

Rishi Pillai is a Senior Research and Development Staff Member and has worked in ORNL's Corrosion Science & Technology Group since 2018. He received his Ph.D. in Materials Science from the Aachen Technical University (RWTH), Aachen, Germany in 2014 and has been conducting high temperature oxidation research since 2008. His main research areas are experimental and computational evaluation of the high temperature behavior of ferritic and austenitic steels, Ni-base alloys and high temperature corrosion/oxidation resistant coatings.

Michael Lance is the Group Leader of the Nuclear Energy Materials Microanalysis Group in the Materials Science and Technology Division at ORNL and is a Senior R&D Staff Member. He received a B.S. in 1992 from Alfred University and an M.S. and PhD from Rutgers University in 1998 in Ceramic Science and Technology. He joined ORNL as a staff member in 1998 and has been active in several research areas including emissions control technologies for diesel engines, high-temperature oxidation and heat exchanger fouling. He performs characterization using Raman spectroscopy, electron microprobe analysis and glow discharge optical emission spectroscopy.

James Keiser is a Distinguished Research and Development Staff Member and has worked in ORNL's Corrosion Science & Technology Group since 1974 where he has studied the compatibility of materials with the environments of energy producing systems. His research has addressed the performance of metallic and ceramic materials in environments containing gaseous, liquid and supercritical corrodents. Several of his current projects concern corrosion issues in biomass and molten halide salts. Dr. Keiser received his B.S. in Materials Science and Ph.D. in Metallurgical Engineering and is a Fellow of NACE International and ASM International.

ABSTRACT

Direct-fired supercritical CO_2 (sCO_2) power cycles are a potential strategy to revolutionize fossil energy as a low-emission power source. To assist in the commercialization of this technology, lower cost steels are needed at ≤650°C in the cycle. However, there is a concern about internal carburization of Fe-based alloys in this environment and the associated embrittlement. Two strategies can be considered: higher alloying additions of Ni and Cr, and coatings that enrich the steel surface with Cr or Al. Generally, thin protective Cr-rich oxide scales appear to prevent C ingress but higher Cr and Ni contents are needed to prevent the formation of Fe-rich oxides. For example, alloy 709 (20Cr-25Ni) showed significantly less C ingress compared to type 316H stainless steel (16Cr-10Ni) at 550°-650°C. Pack aluminized and chromized Gr.91 (9Cr-1Mo) and 316H show some promise. For Cr-rich coatings, carbide formation in the coatings on both alloys in 300 bar sCO_2 at 650°C suggests that their potential is limited to lower temperatures. For Al-rich coatings on Gr.91, it is difficult to form a thin Al-rich oxide with ~20 wt.% Al in the coating at 650°C in 300 bar sCO_2.

INTRODUCTION

As the world searches for clean, dispatchable power generation solutions, the open, direct-fired supercritical CO_2 (sCO_2) Allam cycle could provide the first economical, zero-emission source of electricity from fossil energy [Allam 2013, 2017]. The unique properties of sCO_2 also make it attractive for high-efficiency indirect or closed cycles in nuclear, concentrating solar power (CSP), geothermal, and waste heat recovery [Dostal 2006, Chen 2010, Iverson 2013, Wright 2013, Cheang 2015]. Ten years ago, there was a significant concern if structural materials were sufficiently compatible to enable sCO_2 cycles at >50% efficiency above 700°C, especially with the high impurities expected in the Allam cycle. However, most subsequent studies found that Ni-based alloys were compatible with sCO_2 at up to 800°C [Olivares 2015, 2018; Pint 2015, 2017a, 2017b, 2019, 2020; Mahaffey 2016, Oleksak 2018, 2023]. Nevertheless, because of the low sCO_2 critical point (31°C/7.4 MPa), a considerable portion of the cycle operates at <650°C. For sCO_2-based power cycles to be commercially competitive, lower cost Fe-based materials are needed in the lower temperature components in the cycle. Yet, there is a significant concern about the use of steels in sCO_2 because of prior experience with Grade 9 (Fe-9Cr-1Mo) steel in the UK advanced gas cooled reactors (AGRs) operated with sub-critical 43 bar CO_2 at <550°C where severe internal carburization can occur [Gong 2017]. Studies in the sCO_2 literature have concluded that 9-12%Cr ferritic-martensitic (FM), or sometimes called creep-strength enhanced ferritic (CSEF) steels are limited to 450°C in sCO_2 [Sarrade 2017] and austenitic stainless steels begin to show accelerated reaction kinetics in sCO_2 at 600°C [Furukawa 2011, Tan 2011, Cao 2012, Olivares 2015, Sarrade 2017]. These are lower temperatures than applications in supercritical steam [Shingledecker 2013, Pint 2013] and potentially increases the need for more expensive, Ni-based structural materials to bridge this temperature range.

A multi-year evaluation of sCO_2 performance of steels was undertaken to address this issue and determine the maximum use temperature of representative CSEF and austenitic steels in sCO_2 with and without impurities at 450°-650°C [Pint 2021a, 2022a, 2023a, 2023b, 2023c]. Impurities such as O_2 and H_2O in sCO_2 tend to increase the reaction rate [Mahaffey 2016, Pint 2019, 2022; Oleksak 2023]. The work presented here focuses on the advantages of advanced austenitic steels like alloy 709 and initial results on Cr- and Al-rich coatings on lower alloyed steels. Oxidation-resistant coatings are an obvious potential solution for sCO_2 environments and similar Cr- and Al-rich coatings have been investigated in CO_2 that were beneficial in steam [Lopez 2014, Agüero 2016, Nguyen 2017, Kim 2019, Brittan 2020, Kim 2020, Meissner 2020]. Initial exposures at 650°C reveal the limitations of coatings, especially in impure sCO_2 [Pint 2023a].

EXPERIMENTAL PROCEDURE

Table 1 shows the measured chemical compositions of the structural alloys evaluated in this study. Coupons (~10 x 20 x 1.5mm) and dogbone tensile specimens (SS-3 type: 25.4 mm long, 0.76 x 5 mm gauge) were prepared to a 600 grit SiC finish and ultrasonically cleaned in acetone and methanol prior to exposure. The Cr coatings were made using a proprietary pack cementation commercial process on T91 and 316H substrates. The pack aluminide coatings were fabricated at Tennessee Technological University for 30 min at 1050°C in a pack containing 20wt.% of metal Cr-10wt.%Al powder, 2% NH_4Cl activator and 78% Al_2O_3 filler [Pint 2011]. Exposures in sCO_2 were performed using 500-h cycles. Specimens were exposed in research grade (RG) sCO_2 (<5 ppm O_2, 4.1±0.7 ppm H_2O) in a vertically-oriented autoclave (~266 mm deep x 83 mm inner diameter) machined from alloy 282 with an alloy 282 specimen rack. The autoclave was heated to temperature over several hours (~2°C/min) inside a three-zone furnace at 300 bar with a fluid flow rate of ~2 ml/min. The specimens were held at temperature ±2°C and then cooled in sCO_2 to room temperature. For the controlled impurity experiments, two pumps for sCO_2 and H_2O were used, and O_2 was added as a CO_2–O_2 gaseous mixture from a high pressure cylinder. The O_2 was calculated as 1.0 ± 0.2% and the H_2O content as 0.1 ± 0.05% based on the gas flow rates with the largest variations associated with issues with filters, valves and changing sCO_2 cylinders twice during each 500-h cycle. The low H_2O content is for the reheat cycle after H_2O is removed. Another study investigated higher H_2O contents [Oleksak 2023].

For all of the experiments, the specimens were weighed using a Mettler Toledo model XP205 balance with an accuracy of ~±0.04mg. After exposure, samples were copper plated before being sectioned and mounted for light microscopy and scanning electron microscopy (SEM), TESCAN model MIRA3, equipped with energy dispersive x-ray spectroscopy (EDS). Room temperature tensile tests used a strain rate of 0.015/min per ASTM E8-13. Bulk C was measured using combustion analysis and C profiles (~200-250 μm deep) were measured using GDOES to quantify the C uptake using the initial measured composition in Table 1 as a reference [Lance 2018].

RESULTS AND DISCUSSION

The mass change data for the 300 bar sCO_2, 450°-650°C test matrix for the four steels in Table 1 has been presented previously [Pint 2021, 2022a, 2022b]. Figure 1 summarizes the rate constants

Table 1. Chemical composition of the alloys measured by inductively coupled plasma and combustion analyses in mass%.

Alloy	Fe	Cr	Ni	Mo	Mn	Si	C	Other
T91	88.8	8.6	0.3	0.9	0.46	0.35	0.099	0.2V,0.1Nb,0.045N
VM12	83.3	11.5	0.4	0.4	0.38	0.42	0.120	1.5Co,1.6W,0.2V,0.036N
316H	69.5	16.3	10.0	2.0	0.84	0.46	0.040	0.08V,0.039N,0.02Nb
709	51.3	20.1	25.2	1.5	0.89	0.41	0.064	0.2Nb,0.15N

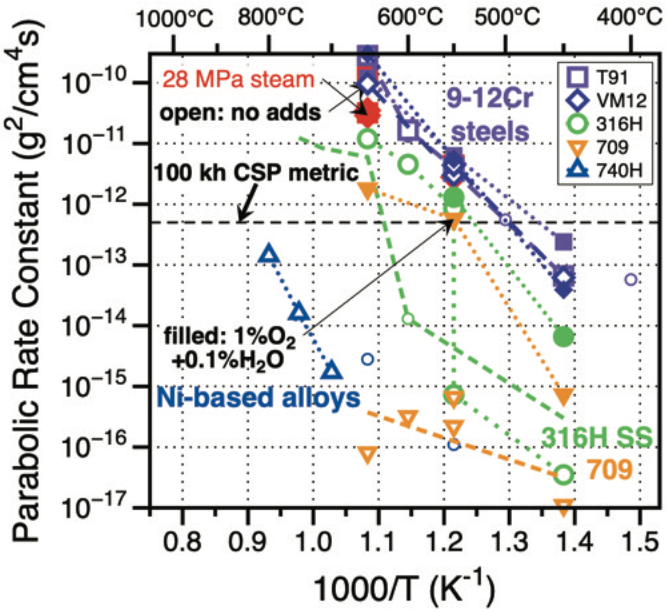

Figure 1. Arrhenius plot of literature values (small circles) and rate constants from this study in 300 bar RG sCO_2 (open symbols) and RG sCO_2+1%O_2+0.1%H_2O (solid symbols) [Pint 2023c].

which were calculated using the median mass change data from 5-6 specimens exposed for 1000-2000 h in each condition using a standard method [Pieraggi 1987]. The open symbols show results for RG sCO_2 and the filled symbols for RG sCO_2 with 1%O_2 and 0.1%H_2O. The horizontal dashed line is a metric developed for 100,000 h CSP applications, with rates below this line not expected to experience significant scale spallation [Pint 2020]. Several values from the literature (open circles) confirm that the rates without impurities are similar to prior work [Furukawa 2011, Dheeradhada 2016]. Rates for Ni-based alloy 740H are well below the metric even at 800°C in RG sCO_2. In some cases the rates are based on only 2 data points (2 cycles, 1000 h total exposure). Prior work showed that rates calculated after 1000 h were similar to those after 10,000 h exposures [Pint 2020].

For the FM/CSEF steels, the rates under these conditions were above the metric for temperatures above ~500°C due to the formation of thick Fe-rich oxides. Figures 2a-2d show example cross-section microstructures after 1,000 h at 650°C with and without impurities. The increased Cr content in VM12 did not significantly affect the rates or oxide morphology under these conditions. As is commonly reported [Furukawa 2011, Tan 2011], these alloys formed duplex Fe-rich oxides in sCO_2. Figure 1 also notes that the rates for T91 and VM12 are similar to those measured after 1000 h in 276 bar H_2O [Pint 2019b]. The key difference in sCO_2 is that C ingress can occur and Figure 3 confirms a significant Increase in bulk C content for both VM12 and T91 at 650°C in RG sCO_2. At 550°C, the C increase is much less but still evident after a 2,000 h exposure (only T91 shown for clarity).

The addition of impurities did slightly increase the rate constant for T91 at 450°C. However, at higher temperatures, minimal changes were observed in the calculated rates. Figures 2a-2d show similar oxides forming with and without impurities on T91 and VM12 at 650°C. The contrast in the light microscopy images does show the formation of Fe_2O_3 with the addition of 1%O_2 which

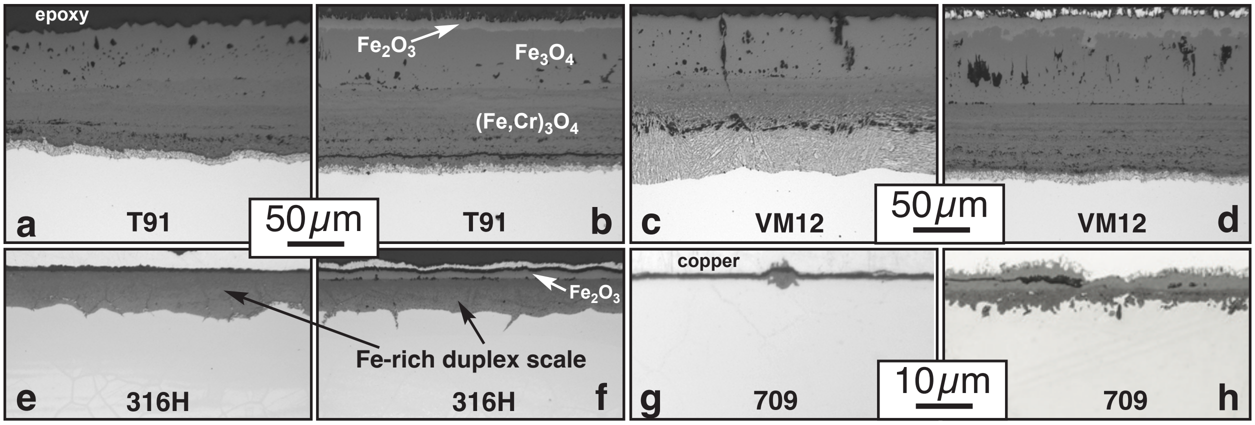

Figure 2. Light microscopy of polished cross-sections after 1,000 h exposures at 650°C in RG sCO_2 (a,c,e,g) without impurities and (b,d,f,h) with 1%O_2 and 0.1%H_2O for (a,b) T91, (c,d) VM12, (e,f) 316H and (g,h) 709.

is consistent with the higher O_2 partial pressure in these experiments. In RG sCO_2, only Fe_3O_4 was observed in the outer layer. In Figure 3, the addition of impurities only slightly increased the C uptake for T91 at 650°C and no increase was noted for VM12.

For 316H and 709, when Cr-rich oxides formed at 450°-550°C in RG sCO_2, the rates were very low, Figure 1. However, impurities did increase the rates due to the formation of Fe-rich oxide nodules [Pint 2022a]. Even without impurities, conventional stainless steels like 316H have been observed to not maintain a protective Cr-rich scale at ≥550°C [Furukawa 2011, Tan 2011]. The increase in rates in Figure 1 is consistent with the formation of Fe-rich oxides and Figures 2e and

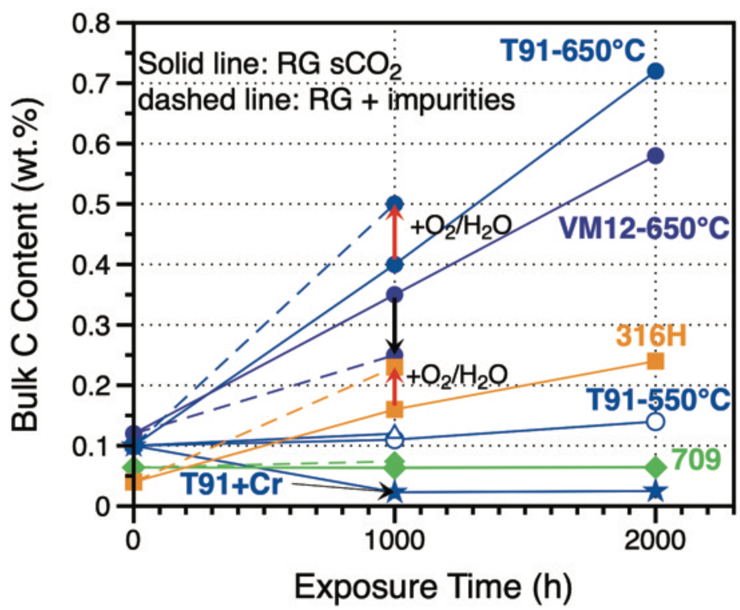

Figure 3. Bulk C content measured as a function of exposure time in sCO_2, closed symbols at 650°C and open symbols at 550°C; solid lines in RG sCO_2 and dashed lines with impurities.

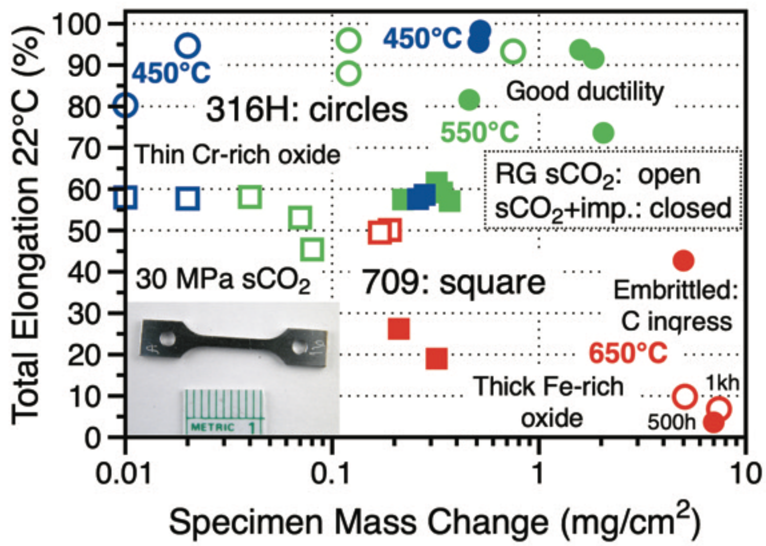

Figure 4: Mass change of 316H and 709 specimens plotted versus post-exposure room temperature total elongation for 500-2000 h exposures in 300 bar RG sCO_2 (open symbols) and RG sCO_2+1%O_2+0.1%H_2O (closed symbols). Compiled data [Pint 2021b,2023c]

2f show mainly the inner layer of Fe-rich oxide formed at 650°C because of the spallation of the outer layer. No rate constant was reported for 316H with impurities at 650°C because of mass loss due to scale spallation. Figure 2f does show an Fe_2O_3 outer layer, similar to the FM steels.

With the formation of a less protective Fe-rich oxide, C ingress was noted for 316H at 650°C, Figure 3. Figure 4 also shows that as the mass gain increases for 316H, the room temperature ductility decreased due to embrittlement. Even with the addition of impurities, the impact on ductility was mainly observed at 650°C. Longer times at lower temperatures could begin to show an effect. Figure 5a shows GDOES results of the C enrichment after sCO_2 exposures at 550° and 650°C. At 650°C, a higher C signal was measured with impurities in the sCO_2, which is

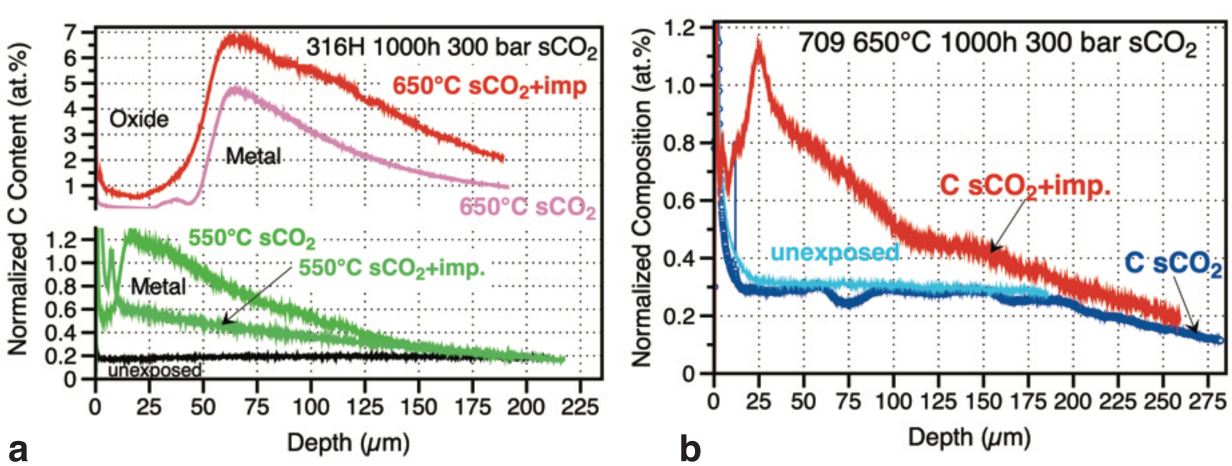

Figure 5. GDOES sputter depth profiles for 1000 h exposures in sCO_2 with and without impurities (a) 316H and (b) 709.

consistent with the bulk measurements in Figure 3. However, a similar increase was not observed at 550°C, Figure 5a.

Now comparing alloy 709 to 316H shows a significant benefit of the higher Cr and Ni contents in alloy 709, Table 1. In RG sCO_2, the rates are lower even at 650°C, where a thin, Cr-rich oxide forms, Figure 2g, even after 2,000 h of exposure. Figure 3 shows no bulk C ingress and Figure 4 shows no decrease in ductility. However, alloy 709 is not immune to the effects of impurities. Figure 2h shows that a duplex scale formed when impurities were added at 650°C. Note that the micron marker for Figures 2g and 2h is different than the other images. However, the higher rates shown in Figure 1 may be capturing a transient effect of Fe-rich oxide formation and not the steady state rate. Nevertheless, impurities disrupted the formation of the thin Cr-rich oxide. Figure 3 shows that after 1,000 h, the bulk C content increased to 0.074% with impurities while no increase in C was observed in RG sCO_2 after 2,000 h. Figure 4 shows that the ductility of alloy 709 specimens decreased from ~50% after exposure in RG sCO_2 at 650°C to <30% after exposure for 500-1000h in RG sCO_2 with impurities. Also, Figure 5b shows a significantly higher C ingress with the addition of impurities. The combination of these results suggests that more work is needed to understand the long-term effects of advanced austenitic steels in impure sCO_2 both in low and high H_2O [Oleksak 2023]. Previously, other highly alloyed austenitic steels, like type 310 stainless steel, showed low C ingress after ≤10,000 h at 750°C [Dryepondt 2022]. The driving force for C ingress is the high C activity at the metal-oxide interface due to the low O_2 partial pressure at the interface [Gheno 2011]. The results for 709 suggest that a thin Cr-rich scale can be an effective C barrier.

Another potential solution for steel sCO_2 compatibility is coatings. Figure 6 summarizes average mass change results after one 500-h cycle at 650°C in RG sCO_2 with and without impurities comparing results for uncoated and coated T91 and 316H. As noted above, very thick Fe-rich oxides form under these conditions on both of these alloys resulting in large mass gains or a mass loss for 316H due to spallation of the outer Fe-rich oxide layer. Starting with chromized T91, the results in RG sCO_2 showed a significant reduction in mass gain, Figure 6. Figures 7a and 7b

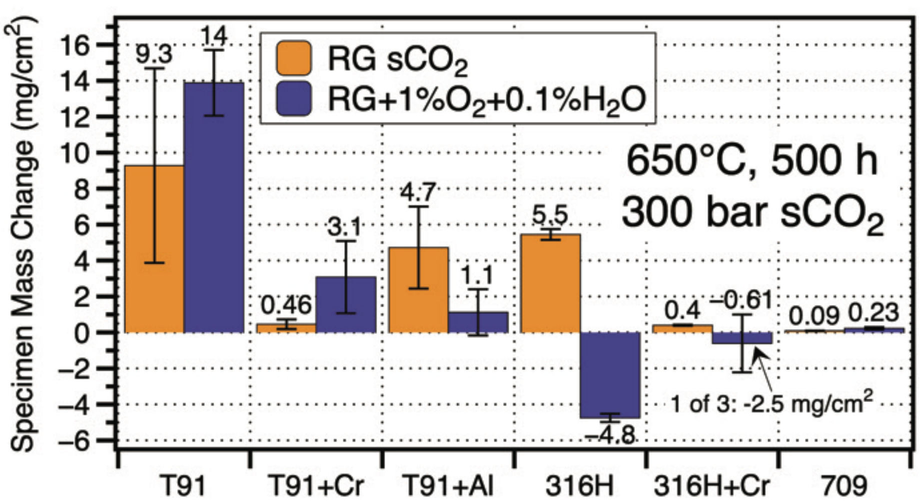

Figure 6. Specimen mass gains during 500-h cycles in 300 bar RG sCO2 after 500 h at 650°C with and without impurities. The whiskers show one standard deviation when multiple specimens were exposed.

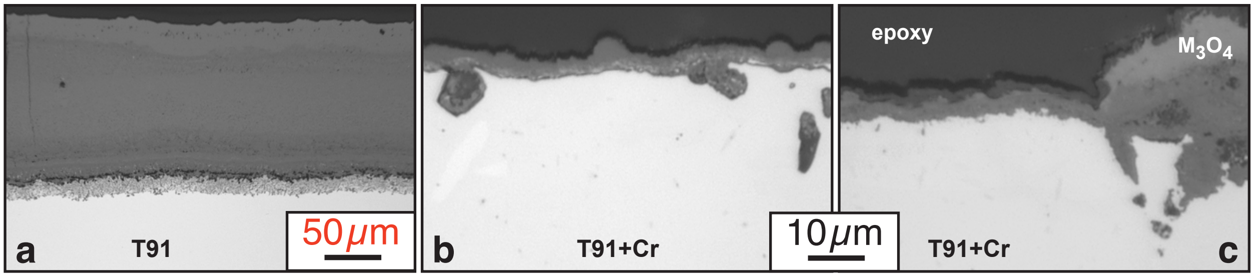

Figure 7. Light microscopy of polished cross-sections of T91 after exposure for 1000 h at 650°C in RG sCO2 (a) uncoated with impurities, (b) chromized without impurities and (c) chromized with impurities.

compares the reaction products on uncoated T91 to the coated specimen. A thin Cr-rich oxide formed after 1,000 h. Small mass gains have been measured for up to 2,000 h in RG sCO_2 at 650°C. Figure 3 also shows no bulk C increase on the coated specimens. However, as documented previously [Pint 2023a], Cr-rich carbides form in the ~100 µm thick coating which ties up the Cr making it less available to form a protective oxide. In the sCO_2 exposures with impurities, the mass gains were higher, Figure 6. Figure 7c shows the formation of Fe-rich oxide nodules, which considerably increases the consumption of Cr from the coating reservoir and suggests that the coating will not remain protective for longer durations.

More recently, Figure 6 also shows results for aluminized T91. However, these results are less

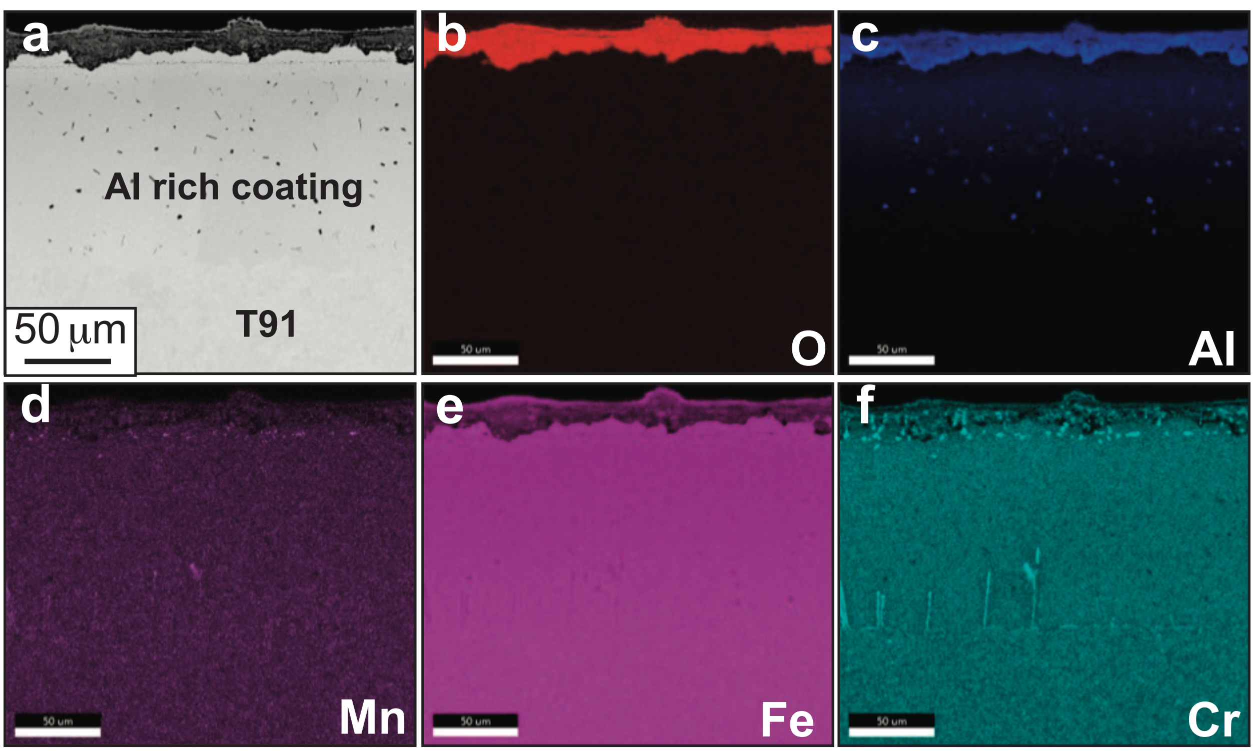

Figure 8. (a) SEM backscattered electron image of aluminized T91 after 500 h at 650°C in RG sCO_2 and (b-f) EDS maps of the same region.

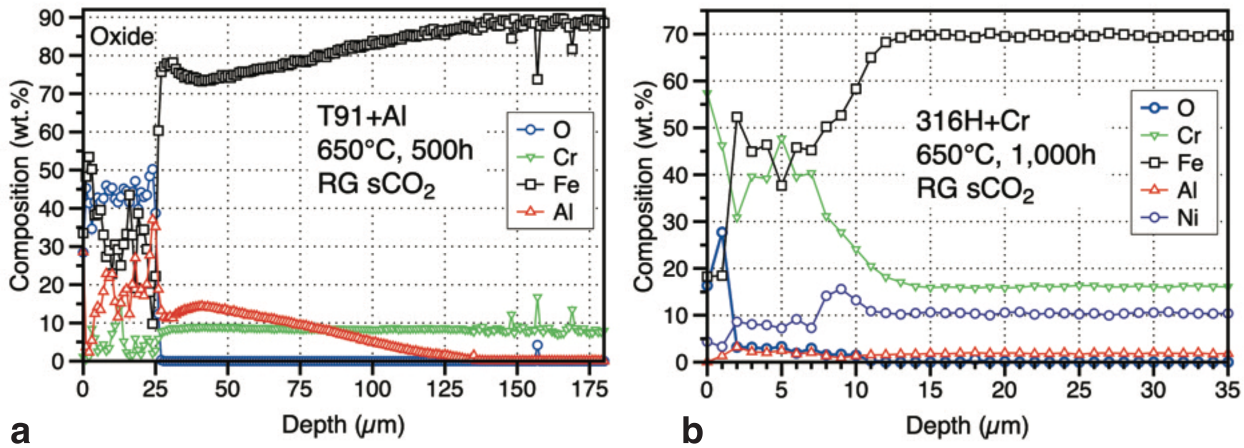

Figure 9. EDS line profiles of the coatings exposed in RG sCO_2 at 650°C (a) aluminized T91 after 500 h (Figure 8) and (b) chromized 316H after 1,000 h (Figure 9).

promising with higher mass gains than chromized T91 in RG sCO_2. The EDS maps in Figure 8 show that a mixed Fe-Al oxide forms rather than Al_2O_3 and the oxide is fairly thick. Figure 9a shows a line profile of the ~25 μm thick oxide and also shows the Al profile in the coating after exposure. The coating had a relatively low Al content in order to minimize the formation of intermetallic aluminide phases which have a higher thermal expansion coefficient than T91 [Pint 2011]. Coatings with a higher Al content may be more effective in sCO_2 at these temperatures.

Finally, chromized 316H also was evaluated and showed similar results as chromized T91 with small mass gains in RG sCO_2. Figure 10 shows the thin Cr-rich oxide scale that formed after 1,000 h. With the slower Cr diffusion in the austenitic 316H substrate compared to T91, the coating in this case was <15 μm thick, Figure 9b. The Cr map in Figure 10c suggests that Cr-rich precipitates also formed in this coating. In Figure 6, this same coating showed mixed results when impurities were added. One specimen of three tested showed a mass loss due to spallation of the reaction product similar to the uncoated alloy. This suggests Fe-rich oxide formation and a less-protective coating in this environment. Coating performance at lower temperatures needs to be evaluated.

CONCLUSIONS

In order to increase the use of less expensive Fe-based alloys in sCO_2 cycles, baseline data has been collected on steels at 450°-650°C in RG sCO_2 to simulate a closed cycle and RG sCO_2 with O_2 and H_2O impurities to simulated the open Allam cycle. The results suggest that conventional FM and austenitic steels may be limited to lower temperatures than used in supercritical steam. However, an advanced austenitic steel, 709, with higher Cr and Ni contents, has performed better in RG sCO_2 and should be further evaluated. When tested in the presence of impurities, 709 specimens formed less protective scales and there was evidence of C ingress which was not apparent without impurities. Several pack cementation coatings were evaluated at 650°C. The Cr-rich coatings on T91 and 316H were able to form a thin Cr-rich oxide after 1,000 h in RG sCO_2, which is a signficant improvement compared to uncoated substrates. However, the formation of Cr-rich precipitates, likely carbides, in the coatings suggests that the long-term durability may be

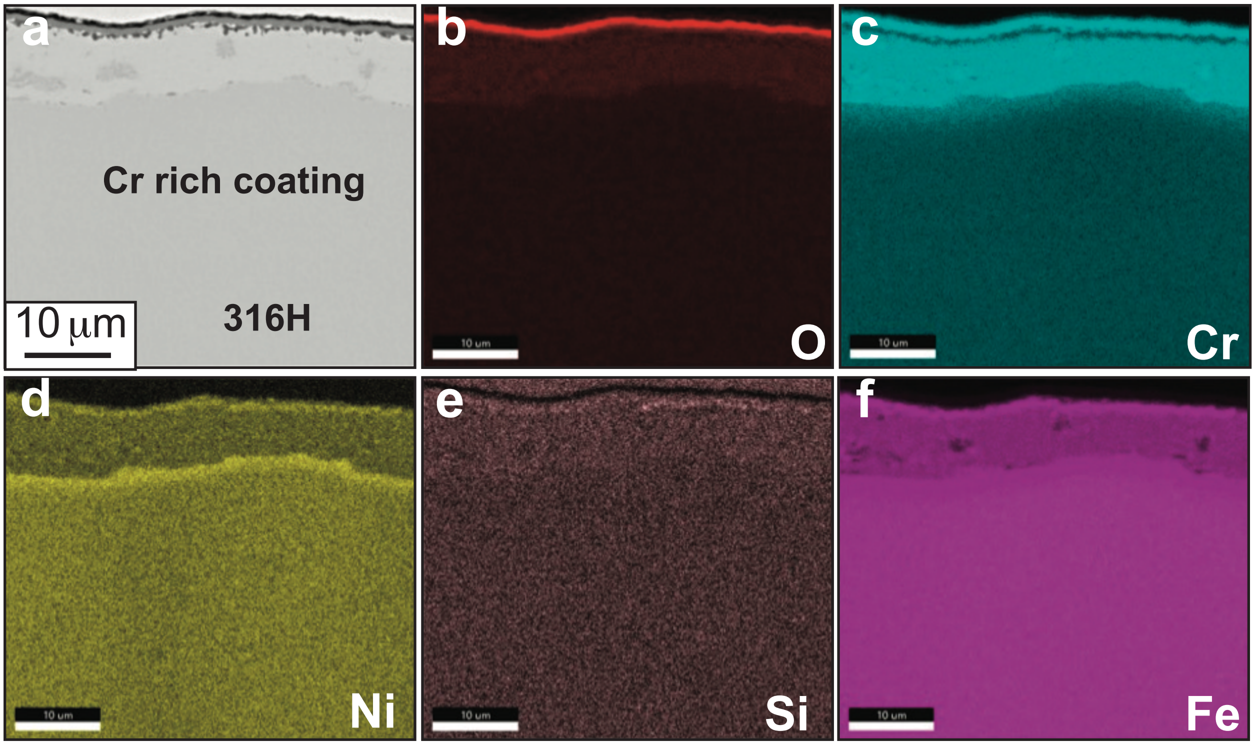

Figure 10. (a) SEM backscattered electron image of chromized 316H after 1,000 h at 650°C in RG sCO_2 and (b-f) EDS maps of the same region

limited. With the addition of impurities in the sCO_2 environment, the coatings did not perform as well including the formation of Fe-rich oxide nodules and faster Cr consumption in the coating. For the pack Al coating, the relatively low, >20wt.%, Al content in the coating was not able to form Al_2O_3 and the mixed Fe-Al oxide was relatively thick.

NOMENCLATURE

CSP	=	Concentrated Solar Power
CSEF	=	Creep strength enhanced ferritic
EDS	=	Energy Dispersive X-ray Spectroscopy
GDOES	=	Glow Discharge Optical Emission Spectroscopy
ORNL	=	Oak Ridge National Laboratory
RG	=	Research Grade
sCO_2	=	Supercritical Carbon Dioxide
SEM	=	Scanning Electron Microscopy
UK	=	United Kingdom

REFERENCES

Agüero, A., Baraibar, I., González, V., Muelas, R., Plana, D., 2016 "Corrosion Resistance of Novel Coatings on Ferritic Steels for Oxycombustion–Supercritical Steam Boilers: Preliminary Results," Oxidation of Metals 85, 263–281.

Allam, R. J., Palmer, M. R., Brown Jr., G. W., Fetvedt, J., Freed, D., Nomoto, H., Itoh, M., Okita, N., Jones Jr., C., 2013, "High efficiency and low cost of electricity generation from fossil fuels while eliminating atmospheric emissions, including carbon dioxide," Energy Procedia 37, 1135–1149.

Allam, R., Martin, S., Forrest, B., Fetvedt, J., Lu, X., Freed, D., Brown, Jr., G. W., Sasaki, T., Itoh, M., Manning, J., 2017, "Demonstration of the Allam Cycle: An Update on the Development Status of a High Efficiency Supercritical Carbon Dioxide Power Process Employing Full Carbon Capture," Energy Procedia 114, 5948-5966.

Brittan, A. M., Mahaffey, J. T., Colgan, N. E., Elbakhshwan, M., Anderson, M. H., 2020, "Carburization resistance of cu-coated stainless steel in supercritical carbon dioxide environments," Corrosion Science 169, 108639.

Cao, G., Firouzdor, V., Sridharan, K., Anderson, M., Allen, T. R., 2012, "Corrosion of austenitic alloys in high temperature supercritical carbon dioxide," Corros. Sci. 60, 246-255.

Cheang, V., Hedderwick, R. A, McGregor, C., 2015, "Benchmarking supercritical carbon dioxide cycles against steam Rankine cycles for Concentrated Solar Power," Solar Energy, 113, 199-211.

Chen, H., Goswami, D. Y., Stefanakos, E. K., 2010, "A review of thermodynamic cycles and working fluids for the conversion of low-grade heat," Renewable & Sustainable Energy Reviews 14, 3059-3067.

Dheeradhada, V., Thatte, A., Karadge, M., Drobnjak, M., 2016, "Corrosion of Supercritical CO_2 Turbomachinery Components," in Proceedings of the EPRI International Conference on Corrosion in Power Plants, Oct. 2016, San Diego, CA.

Dostal, V., Hejzlar, P., Driscoll, M. J., 2006, "The supercritical carbon dioxide power cycle: Comparison to other advanced power cycles," Nuclear Technology, 154(3), 283-301.

Dryepondt, S., Lehmusto, J., Pint, B. A., 2022, "Effect of Annealing and Supercritical CO_2 Exposure at 750 °C on the Tensile Properties of Stainless Steel and Ni-based Structural Alloys," Materials and Corrosion 73, 497-512.

Furukawa, T., Inagaki, Y., Aritomi, M., 2011, "Compatibility of FBR structural materials with supercritical carbon dioxide," Progress in Nuclear Energy 53, 1050–1055.

Gheno, T., Monceau, D., Zhang, J., Young, D. J., 2011 "Carburisation of Ferritic Fe-Cr Alloys by Low Carbon Activity Gases," Corrosion Science 53, 2767-2777.

Gong, Y., Young, D. J., Kontis, P. Chiu, Y. L., Larsson, H., Shin, A., Pearson, J. M., Moody, M. P., Reed, R. C., 2017, "On the breakaway oxidation of Fe9Cr1Mo steel in high pressure CO_2," Acta Materialia, 130, 361-374.

Iverson, B. D., Conboy, T. M., Pasch, J. J., Kruizenga, A. M., 2013, "Supercritical CO_2 Brayton cycles for solar-thermal energy," Applied Energy, 111, 957-970.

Kim, C., Kim, S. H., Cha, J.-H., Jang, C., Kim, T. K., 2019, "Cr diffusion coating to improve the corrosion resistance of an ODS steel in super-critical carbon dioxide environment," Surface and Coatings Technology 374, 666-673.

Kim, S. H., Kim, C., Cha, J.-H., Jang, C., 2020, "Corrosion Behavior of Si Diffusion Coating on an Austenitic Fe-Base Alloy in High Temperature Supercritical-Carbon Dioxide and Steam Environment," Coatings 10, 493.

Lance, M. J., Leonard, D. N., Pint, B. A., 2018, "The Use of Glow Discharge Optical Emission Spectroscopy to Quantify Internal Carburization in Supercritical CO_2," in Proceedings of the 6th International Symposium on Supercritical CO_2 Power Cycles, Pittsburgh, PA, Paper #117.

López, A. J., Proy, M., Utrilla, V., Otero, E., Rams, J., 2014, "High-temperature corrosion behavior of Ni–50Cr coating deposited by high velocity oxygen–fuel technique on low alloy ferritic steel," Materials and Design 59, 94–102.

Mahaffey, J., Adam, D., Brittan, A., Anderson, M., Sridharan, K., 2016, "Corrosion of Alloy Haynes 230 in High Temperature Supercritical Carbon Dioxide with Oxygen Impurity Additions," Oxidation of Metals 86, 567-580.

Meissner, T. M., Gregoire, B., Montero, X., Miller, E., Maier, J., Galetz, M. C., 2020 "Long-Term Corrosion Behavior of Cr Diffusion Coatings on Ferritic-Martensitic Superheater Tube Material X20CrMoV12-1 under Conditions Mimicking Biomass (Co-)firing," Energy & Fuels 34, 10989-11002.

Nguyen, T. D., Peng, X., Zhang, J. Q., Young, D. J., 2017, "Corrosion resistance of chromised and aluminised coatings in wet CO_2 gas at 650°C," Surface and Coatings Technology 316, 226–238.

Oleksak, R. P., Tylczak, J. H., Carney, C. S., Holcomb, G. R., Dogan, O. N., 2018, "High-Temperature Oxidation of Commercial Alloys in Supercritical CO_2 and Related Power Cycle Environments," JOM 70, 1527-1534.

Oleksak, R. P., Carney, C. S., Dogan, O. N., 2023, "Effect of pressure on high-temperature oxidation of Ni alloys in supercritical CO_2 containing impurities," Corrosion Science 215, 111055.

Olivares, R. I., Young, D. J., Marvig, P., Stein, W., 2015, "Alloys SS316 and Hastelloy-C276 in Supercritical CO_2 at High Temperature," Oxid. Met. 84, 585–606.

Olivares, R. I., Young, D. J., Nguyen, T. D., Marvig, P., 2018, "Resistance of High-Nickel, Heat-Resisting Alloys to Air and to Supercritical CO_2 at High Temperatures," Oxid. Met. 90, 1-25.

Pieraggi, B., 1987, "Calculations of Parabolic Reaction Rate Constants," Oxid. Met. 27, 177-185.

Pint, B. A., Zhang, Y., 2011, "Performance of Al-rich Oxidation Resistant Coatings for Fe-Base Alloys," Mater. Corros. 62, 549-560.

Pint B. A., 2013, "High-Temperature Corrosion in Fossil Fuel Power Generation: Present and Future," JOM 65, 1024-1032.

Pint B. A., Keiser, J. R., 2015, "Initial Assessment of Ni-Base Alloy Performance in 0.1 MPa and Supercritical CO_2," JOM 67(11), 2615-2620.

Pint B. A., Brese, R. G., 2017a, "High-Temperature Materials," in Fundamentals and Applications of Supercritical Carbon Dioxide Based Power Cycles, K. Brun and P. Friedman, eds., Elsevier, London, pp.67-104.

Pint, B. A., Brese, R. G., Keiser, J. R., 2017b, "Effect of Pressure on Supercritical CO_2 Compatibility of Structural Alloys at 750°C," Mater. Corros. 68, 151-158.

Pint, B. A., Lehmusto, J., Lance M. J., Keiser, J. R., 2019a, "The Effect of Pressure and Impurities on Oxidation in Supercritical CO_2," Mater. Corros. 70, 1400-1409.

Pint, B. A., Pearson, S. R., De Las Casas Aranda, R., Lance, M. J., Raiman, S. S., Kung, S. C., 2019b, "Water Chemistry and Pressure Effects on Steam Oxidation of Ferritic and Austenitic Steels," in Proceedings of the Joint EPRI – 123HiMAT International Conference on Advances in High Temperature Materials, J. Shingledecker and M. Takeyama eds., ASM International, Materials Park, OH, pp.939-947.

Pint, B. A., Pillai, R., Lance M. J., Keiser, J. R., 2020, "Effect of Pressure and Thermal Cycling on Long-Term Oxidation in CO_2 and Supercritical CO_2" Oxid. Met. 94, 505–526.

Pint, B. A., Pillai, R., Keiser, J. R., 2021a "Effect of Supercritical CO_2 on Steel Ductility at 450°-

650°C” ASME Paper #GT2021-59383, for Turbo Expo 2021 Virtual Conference and Exhibition, June 11-15, 2021.

Pint, B. A., 2021b, “High temperature compatibility of structural alloys with supercritical and subcritical CO_2,” Interface 30, 67-71

Pint, B. A., Lance M. J., Pillai, R., Keiser, J. R., 2022a “Compatibility of Steels at 450°-650°C in Supercritical CO_2 with O_2 and H_2O Additions” NACE Paper C2022-18018, Houston, TX, presented at Corrosion 2022, San Antonio, TX.

Pint, B. A., Pillai, R., Keiser, J. R., 2022b “Defining Temperature Limitations for Steels in sCO_2 Applications,” in Proceedings of the 7th International Symposium on Supercritical CO2 Power Cycles, San Antonio, TX, February 2022, Paper #38.

Pint, B. A., Pillai, R., Keiser, J. R., 2023a, “Evaluation of Coatings to Improve Steel Compatibility in Supercritical CO_2” AMPP Paper C2023-19207, Houston, TX, to be presented at AMPP Annual, March 2023, Denver, CO.

Pint, B. A., Su, Y.-F., Lance M. J., Pillai, R., Keiser, J. R., 2023b, “Internal Carburization and Scale Formation on Austenitic Steels in Supercritical Carbon Dioxide,” Mater. High Temp. 40, 308-317.

Pint, B. A., Lance M. J., Pillai, R., Keiser, J. R., 2023c, “Effect of Impurities on the Compatibility of Steels in Supercritical CO_2 at 450°-650°C,” ASME Paper #GT2023-103838, for Turbo Expo 2023 Conference and Exhibition, June 26-30, 2023.

Sarrade, S., Férona, D., Rouillard, F., Perrin, S., Robin, R., Ruiz, J.-C., Turc, H.-A., 2017, “Overview on corrosion in supercritical fluids,” J. of Supercritical Fluids 120 (2017) 335–344.

Shingledecker, J. P., Pint, B. A., Sabau, A. S., Fry, A. T., Wright, I. G., 2013, “Managing Steam-Side Oxidation and Exfoliation in USC Boiler Tubes,” Adv. Mater. Processing 171 (1), 23-25.

Tan, L. Anderson, M., Taylor, D., Allen, T. R., 2011, “Corrosion of austenitic and ferritic-martensitic steels exposed to supercritical carbon dioxide,” Corros. Sci. 53, 3273-3280.

Wright, I. G., Pint, B. A., Shingledecker, J. P., Thimsen, D., 2013, “Materials Considerations for Supercritical CO_2 Turbine Cycles,” ASME Paper #GT2013-94941, presented at the International Gas Turbine & Aeroengine Congress & Exhibition, San Antonio, TX, June, 3-7, 2013.

ACKNOWLEDGMENTS

The authors would like to thank B. Johnston, A. Willoughby and D. Newberry at ORNL for assistance with the experimental work. Material was provided by Tenaris, EPRI and S. Sham at INL and Y. Wang at ORNL. J. Jun and Y.-F. Su at ORNL provided helpful comments on the manuscript. This research was sponsored by the U.S. Department of Energy, Office of Fossil Energy and Carbon Management, Advanced Materials Program. This manuscript has been authored by UT-Battelle, LLC under Contract No. DE-AC05-00OR22725 with the U.S. Department of Energy. The United States Government retains and the publisher, by accepting the article for publication, acknowledges that the United States Government retains a non-exclusive, paid-up, irrevocable, world-wide license to publish or reproduce the published form of this manuscript, or allow others to do so, for United States Government purposes. The Department of Energy will provide public access to these results of federally sponsored research in accordance with the DOE Public Access Plan (http://energy.gov/downloads/doe-public-access-plan).